# Variations in the colchicine-binding domain provide insight into the structural switch of tubulin

Audrey Dorléans[a,1], Benoît Gigant[a], Raimond B. G. Ravelli[b], Patrick Mailliet[c], Vincent Mikol[c], and Marcel Knossow[a,2]

[a]Laboratoire d'Enzymologie et Biochimie Structurales, Centre National de la Recherche Scientifique, Bâtiment 34, 1, avenue de la Terrasse, 91198 Gif sur Yvette, France; [b]Leiden University Medical Center, P.O. Box 9600, 2300 RC Leiden, The Netherlands; and [c]Research and Development, Sanofi-Aventis, 13 Quai J. Guesde, 94403 Vitry sur Seine, France

Edited by J. Richard McIntosh, University of Colorado, Boulder, CO, and approved June 17, 2009 (received for review April 17, 2009)

**Structural changes occur in the αβ-tubulin heterodimer during the microtubule assembly/disassembly cycle. Their most prominent feature is a transition from a straight, microtubular structure to a curved structure. There is a broad range of small molecule compounds that disturbs the microtubule cycle, a class of which targets the colchicine-binding site and prevents microtubule assembly. This class includes compounds with very different chemical structures, and it is presently unknown whether they prevent tubulin polymerization by the same mechanism. To address this issue, we have determined the structures of tubulin complexed with a set of such ligands and show that they interfere with several of the movements of tubulin subunits structural elements upon its transition from curved to straight. We also determined the structure of tubulin unliganded at the colchicine site; this reveals that a β-tubulin loop (termed T7) flips into this site. As with colchicine site ligands, this prevents a helix which is at the interface with α-tubulin from stacking onto a β-tubulin β sheet as in straight protofilaments. Whereas in the presence of these ligands the interference with microtubule assembly gets frozen, by flipping in and out the β-subunit T7 loop participates in a reversible way in the resistance to straightening that opposes microtubule assembly. Our results suggest that it thereby contributes to microtubule dynamic instability.**

cytoskeleton | inhibitors | microtubules

Microtubules are hollow cylindrical assemblies of αβ-tubulin heterodimers (tubulin). They participate in numerous processes such as cell division, where they form the mitotic spindle, or intracellular trafficking, where they constitute the roads along which microtubule-based motors move. To fulfill their wide range of functions, microtubules alternate phases of growth and shrinkage in a process known as dynamic instability (1). The assembly-disassembly cycle is accompanied by a nucleotide cycle, which is well understood. To be competent for polymerization, tubulin should be in a GTP state, i.e., with GTP bound to the β-subunit (the GTP molecule bound to α is neither hydrolyzed nor exchanged). GTP hydrolysis accompanies microtubule assembly, and GDP-tubulin is released upon disassembly (2). Tubulin also undergoes a structural cycle that is deciphered only in part. Structural data have been obtained on GDP-tubulin, either assembled in sheets of straight protofilaments mimicking the microtubule state (3) or in a curved protofilament-like complex of 2 tubulins with the stathmin-like domain (SLD) of the RB3 protein (RB3-SLD) (4). This structure has provided an atomic model for a conformation of unpolymerized tubulin, revealing that the overall curvature of the complex is due to reorientations of neighboring tubulin subunits with respect to each other both within a heterodimer and at the interheterodimer interface. These orientation changes accommodate variations at the intersubunit contact surfaces due to rearrangements of tubulin domains with respect to the structure in straight protofilaments (4).

In the structure of unassembled tubulin (4), the bound nucleotide is GDP and the protein is complexed to colchicine, a small molecule ligand which is located in β-tubulin, at the interface with the α-subunit of the same heterodimer. Tubulin-colchicine gets incorporated in microtubules to a very limited extent whatever the nucleotide (5), which means that structural changes that occur in tubulin-colchicine and prevent its incorporation in microtubules become frozen after ligand binding. This differs from changes in GDP-tubulin compared with GTP-tubulin which also prevent microtubule assembly but whose effects may be reversed (6). These observations raise 2 questions. First, what are the molecular mechanisms that prevent the domain movements required to go from curved to straight tubulin when there is a ligand at the colchicine site? Second, is the arrangement of the 2 subunits of soluble GDP-tubulin curved in the absence of colchicine and, if this is the case, what gives rise to this curvature and how is it reversed?

We report here atomic structures of complexes of 2 tubulins with the RB3-SLD ($T_2R$) that address these issues. In the first structure, there is no exogenous inhibitor bound to tubulin in the colchicine site. This allows us to identify local changes that account for tubulin curvature in the absence of any colchicine site ligand. In addition, we compare structures of $T_2R$ where tubulin is complexed to colchicine and to three other ligands with significantly different chemical formulas (Fig. 1), taking advantage of the wide variety of ligands that target the colchicine site. This defines molecular mechanisms that prevent the tubulin transition from curved to straight.

## Results

**Structure of the $T_2R$ Complex with No Exogenous Ligand Bound.** The stabilization of tubulin through SLD binding has proven successful to obtain structural information on this fragile protein. However, we have long been unable to describe differences between tubulin with an empty and an occupied colchicine site, because of the too low resolution of diffraction by empty $T_2R$ crystals. Successive incremental improvements including optimization of the crystallization temperature (7) resulted in $T_2R$ crystals that diffracted to 3.65 Å resolution (Table S1). The unliganded complex remains curved, and its curvature is unchanged compared with colchicine-bound $T_2R$, the only structural differences being local. Their main feature is a switch of the T7 loop (tubulin secondary structure elements are presented in Figs. 2–4; for their localization in the sequence and for tubulin residue numbering, see reference 3

Author contributions: A.D., B.G., V.M., and M.K. designed research; A.D., B.G., and R.B.G.R. performed research; P.M. contributed new reagents/analytic tools; A.D., B.G., V.M., and M.K. analyzed data; and A.D., B.G., R.B.G.R., V.M., and M.K. wrote the paper.

Conflict of interest statement: P.M. and V.M. are employees of the company that sells Taxotere, an anti-cancer drug that targets tubulin.

This article is a PNAS Direct Submission.

[1]Present address: Institut de Biologie Physico-Chimique, Centre National de la Recherche Scientifique, 13, rue Pierre et Marie Curie, 75005 Paris, France.

[2]To whom correspondence should be addressed. E-mail: knossow@lebs.cnrs-gif.fr.

This article contains supporting information online at www.pnas.org/cgi/content/full/0904223106/DCSupplemental.

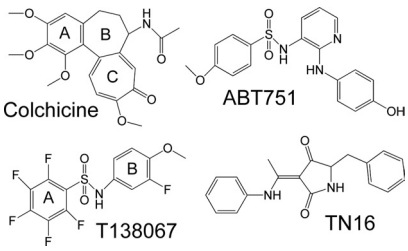


**Fig. 1.** Chemical formulas of colchicine and of the three colchicine domain compounds used in this study.

and the legends to Figs. 2 and 3). In the absence of a ligand, this loop lies in the colchicine site, the side chain of residue Asn β249 overlapping with the colchicine A ring when the corresponding structures are superimposed (Fig. 2). The T7 loop flips to make room for the ligand. This is likely to be a fast process and does not account for the well-documented slow binding of colchicine (8), as it also occurs when other colchicine site ligands bind to tubulin. Most of these do not present any peculiar association kinetics. The T7 loop links helix H8 to the central helix H7. The latter undergoes a translation when tubulin converts from a straight to a curved state (4). When tubulin is embedded in a microtubule, this loop mediates longitudinal contacts with the neighboring monomer and in particular with its nucleotide (9). Therefore, the T7 loop adopts at least 3 different conformations according to the assembly state and to the presence of an exogenous molecule in the colchicine site.

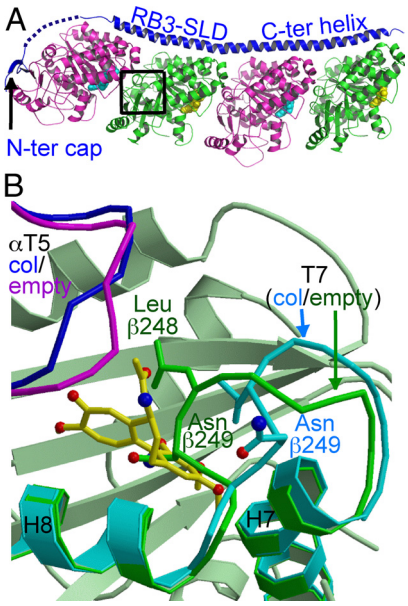


**Fig. 2.** The conformations of the β-subunit T7 loop in soluble tubulin. (*A*) Overview of $T_2R$, with the α-subunits in magenta (with bound GTP in cyan), β-subunits in green (GDP in yellow), and RB3-SLD in blue. The linker between the RB3-SLD N-terminal cap (labeled N-ter cap) and its C-terminal helix is disordered and shown as a dotted line. The colchicine-binding site, presented in *B*, is framed; there is an identical site at the other αβ interface. (*B*) The switch of the T7 loop upon colchicine binding. The β-subunit without any ligand at the colchicine site (PDB ID code: 3HKB) is in green. The T7 loop (residues 244–251) of the β-subunit with bound colchicine (yellow) is presented together with helices H7 (residues 224–243) and H8 (residues 252–260), in cyan. For clarity, only the T5 loop of the α-subunit is drawn (residues 173–182). Electron density maps of loop T7 in the unliganded structure are presented in Fig. S3.

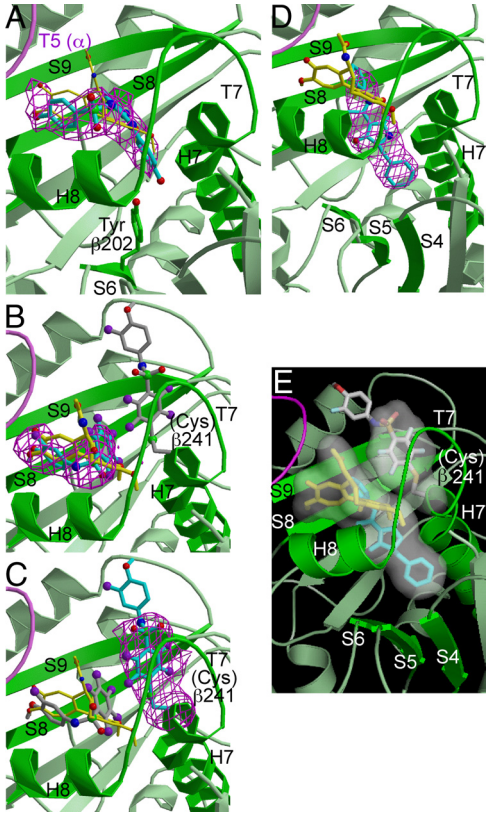


**Fig. 3.** The colchicine domain. The ligands bound to $T_2R$ are presented in cyan in their respective Fobs-Fcalc omit maps contoured either at 3 σ (*A* and *C*) or at 3.5 σ (*B* and *D*) and overlapped with colchicine (yellow). For clarity, only the T5 loop of the α-subunit is drawn (magenta). Secondary structure elements presented are defined as follows: S4 (residues 134–140), S5 (166–171), S6 (200–204), S8 (313–320), and S9 (351–356). (*A*) ABT751 (PDB ID code: 3HKC). (*B* and *C*) The 2 binding modes of T138067 (PDB ID code: 3HKE). The position overlapping with colchicine is presented in its electron density in *B*; that same position is in gray in *C*. A ligand covalently bound to Cys β241 is presented in its electron density in *C* (reversed colors). (*D*) TN16 (PDB ID code: 3HKD). (*E*) The volume occupied by colchicine domain ligands. The overlapping surfaces of colchicine and TN16 are drawn together with that of the ordered part of covalently bound T138067. They are superimposed with colchicine (yellow), TN16 (cyan), and modified Cys β241 (gray).

**Extending the Definition of the Colchicine Site: The Colchicine Domain.** Tubulin is the target of numerous small molecule inhibitors. Most of them bind to one of the three characterized tubulin ligand sites, the taxol, vinca, and colchicine sites. Each of them accommodates compounds with very different structures (10). We determined the structures of $T_2R$ in complex with 3 such compounds (Table S1) that all differ significantly from colchicine (Fig. 1) and prevent microtubule assembly (11–13). All compounds establish very few polar interactions with tubulin, making mostly van der Waals contacts with it. Two of them colocalize with colchicine, they will be presented in the two following sections. The binding site of the third one overlaps only in part with that of colchicine, it defines an extension of this site and will be presented in a later section.

***Structure of the $T_2R$-ABT751 complex.*** ABT751, also named E7010, is a synthetic sulfonamide molecule currently evaluated as an anti-cancer drug (14) (Fig. 1). We have determined the $T_2R$-ABT751 structure at 3.8 Å resolution. The ligand orientation in its tubulin site was confirmed with the use of a bromo-derivative (see *Materials and Methods*) (Fig. 3*A* and Fig. S1). As expected from competition experiments (13), ABT751 binds to the colchicine site. When the β-subunits in the $T_2R$-colchicine and

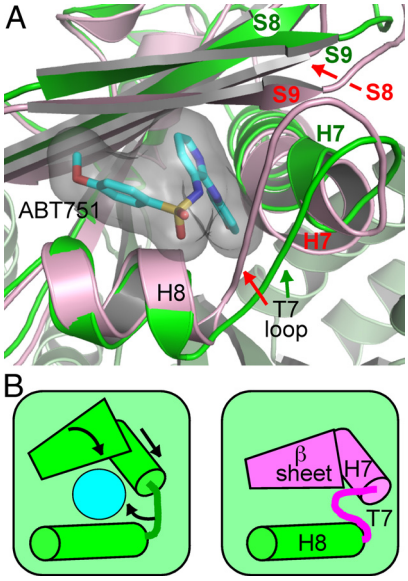


**Fig. 4.** Structural changes in the colchicine domain upon tubulin conversion from curved to straight. (*A*) One β-subunit of tubulin in $T_2$R-ABT751 is shown in pale green (N-terminal domain and C-terminal helices) and darker green (intermediate domain, from H6 to S10). ABT751 is in cyan. The intermediate domain of β-tubulin in its straight conformation (PDB ID: 1JFF) is depicted (pink) after superposition of the N-terminal domain on that of β-tubulin in $T_2$R. In the straight structure, the intermediate domain β sheet, in particular strands S8 and S9, comes closer to the H8 helix. Together with the H7 translation, this leads to a shrinking of the colchicine domain. When a ligand is bound to it, the straight conformation cannot be accommodated owing to steric clashes with surrounding secondary structure elements (S8, S9, H7, and H8). A stereoscopic view of this Figure is presented in Fig. S4. (*B*) Schematic view of the conversion from curved (*Left*) to straight tubulin (*Right*). Movements of tubulin intermediate domain secondary structure elements are indicated by arrows. These movements are prevented by colchicine domain ligands (represented here as a blue disk).

$T_2$R-ABT751 complexes are superimposed, the electron density envelopes of these ligands largely coincide. The methoxy benzene and pyridine groups of ABT751 superimpose with the colchicine C and A rings, respectively, while the sulfonamide linker overlaps with the B ring (Fig. 3*A*). Nevertheless ABT751 is more deeply buried than colchicine in β-tubulin. This has 2 consequences. First, in addition to the secondary structure elements of the tubulin intermediate domain contacted by colchicine, ABT751 interacts with strand S6 of the N-terminal nucleotide binding domain, mainly through contacts between the hydroxyaminophenyl group and residue Tyr β202. Second, ABT751 does not interact with the α-subunit, as opposed to colchicine, which contacts the α-tubulin T5 loop through its N-acetyl substituent. This loop has been shown to adopt 2 alternate conformations, depending on the colchicine site ligand (4, 15). The conformation adopted in $T_2$R-ABT751 is the same as in the $T_2$R-podophyllotoxin complex (4) and as in empty $T_2$R.

***Structure of the $T_2$R-T138067 complex: A dual binding mode with a covalent component.*** T138067 is a polycyclic molecule comprising 2 rings and sharing with ABT751 a sulfonamide linker (Fig. 1). It binds covalently to residue Cys 241 of β-tubulin (12) (Cys 241 is the 239th residue of the β chain; residue numbering is chosen to be consistent with that of α-tubulin and with previous tubulin structural work). The 3.6 Å resolution electron density maps of the $T_2$R-T138067 complex reveal a dual binding mode. Some of the ligand molecules occupy a site largely overlapping with that of colchicine while others are covalently linked to Cys β241 (Figs. 3*B* and *C*). In the latter case, only ring A, bound to Cys β241, and the sulfonamide moiety are visible in the electron density; they interact mainly with strand S9 and loop T7, that border the colchicine site on the α-tubulin side. Ring B is disordered and points toward the solvent. Occupancy refinement of the 2 ligand populations leads to an occupancy of the noncovalently bound one between 0.7 and 1, while that of the covalently bound one is between 0.6 and 0.8. This is consistent with the nature of the β241 residue, which depends on the isotype. It is a serine in βIII tubulin, which amounts to 25% of mammalian brain tubulin (16), and a cysteine in other isotypes. As the overall occupancy is higher than unity, the 2 binding modes are not exclusive of each other. This is supported by the structure as there is no disallowed interference in $T_2$R in which 2 T138067 molecules are modeled in the same β-subunit. Moreover, some stabilization may arise from the stacking of the A ring of the covalently bound molecule with that of the noncovalently bound one.

***The $T_2$R-TN16 complex: Extension of the colchicine site.*** TN16 (Fig. 1) has long been recognized as an inhibitor of microtubule assembly that competes with colchicine for tubulin binding (11). Inspection of the 3.7 Å Fobs-Fcalc electron density map of $T_2$R-TN16 shows that the overlap of the TN16 binding site with the colchicine site is limited to the subsite accommodating the colchicine A ring (Fig. 3*D*). TN16 is even more deeply buried in the β monomer than the ABT751 ligand. As a consequence, it makes fewer contacts with the secondary structure elements of the tubulin intermediate domain while establishing new interactions with the nucleotide-binding domain. The tubulin residues involved belong to β strands S4, S5, and S6 in this domain. The orientation of the TN16 molecule we propose is based on the best fit in its Fobs-Fcalc and 2Fobs-Fcalc omit maps and optimizes polar interactions with tubulin, but, owing to the cylindrical shape of the electron density, alternate orientations cannot be excluded.

The structures we determined lead us to propose that ligands competing with colchicine for tubulin binding bind to a "colchicine domain" which consists of a main site and of additional pockets (Fig. 3*E*). The main site accommodates most of the ligands whose interaction with tubulin has been structurally characterized, namely colchicine, podophyllotoxin, as well as ABT751 and noncovalently bound T138067 (ref. 4 and this work). The additional pockets are either buried deeper in the β-subunit, as revealed by TN16, or extend from the Cys β241 side-chain (covalently bound T138067). This situation is similar to that of the tubulin vinca domain that may be described as consisting of a core targeted by all ligands that interfere with vinblastine for tubulin binding and of ligand-dependent extensions (17). Extensions of the colchicine-binding site of smaller amplitude than that occupied by TN16 were previously suggested based on modeling (18). Our result provides an experimental basis to guide the design of antimitotic agents that target the whole colchicine domain.

## Discussion

Tubulin undergoes structural changes along its microtubule assembly/disassembly cycle. These consist in variations within tubulin subunits that affect in particular their longitudinal interfaces (those at contacts between subunits in protofilaments or protofilament-like assemblies) as well as in orientation changes of the subunits that accommodate these variations. To identify the factors that may keep soluble tubulin in a curved conformation, we compared the structures of tubulin in Zn-sheets straight protofilaments and in $T_2$R (with or without colchicine, since this does not affect the structure except in the colchicine neighborhood). While Zn-sheets protofilaments reflect the arrangement of tubulins along the microtubule axis, some changes in the subunits are expected since the lateral interactions between protofilaments in the 2 assemblies differ. Indeed, adaptations of the M loop and of the H6 helix were reported (19). The question of the similarity of

GDP-tubulin in solution and in $T_2R$ also arises. Although some local differences must exist in this case too, there is substantial evidence that RB3-SLD does not affect significantly the tubulin surfaces that are at longitudinal interfaces in $T_2R$. This relates to the contacts of RB3-SLD with tubulin. Two regions may be distinguished in RB3-SLD: its N-terminal part, which caps $T_2R$ (4), and its long C-terminal helix. The RB3-SLD N-terminal peptide is distant by ≈40 Å from the closest intersubunit longitudinal interface (Fig. 2*A*). The RB3-SLD C-terminal helix only contacts residues in the nucleotide binding domain and in the C-terminal helical hairpin (20), an ensemble that is unchanged in $T_2R$ with respect to straight protofilaments [root mean square deviation (r.m.s.d.) of Cα positions: 0.8 Å, within the range expected for identical structures, given the resolution of the corresponding diffraction data]. Therefore, the main function of the RB3-SLD C-terminal helix is to hold tubulin heterodimers together in $T_2R$ in relative orientations that are consistent with low resolution images of curved tubulin assemblies that do not comprise RB3-SLD and are obtained with or without colchicine (20). We summarize here the movements within subunits that give rise to the subunits orientation changes on going from a curved to a straight assembly.

Taking the ensemble of the N-terminal nucleotide-binding domain together with the C-terminal helical hairpin as a reference, a major change concerns the intermediate domain whose β sheet rotates, placing the M loop in a position to mediate lateral contacts with the neighboring protofilament. In addition, for a tubulin subunit to establish microtubular longitudinal contacts with its 2 neighbors, its H6 helix and the following loop stack onto the monomer (4). This is accompanied by a translation of the H7 helix, which runs all along the longitudinal axis of the tubulin subunit. On the other side of the monomer, the T7 loop, which is immediately C-terminal to helix H7, stacks onto the β sheet of the intermediate domain. The H8 helix, which is immediately downstream of the T7 loop and is embedded in the intermediate domain sequence, does not move much (see Fig. 4; the r.m.s.d. of its Cαs after superposition of the N-terminal domains is 1 Å, over 9 residues, much smaller than the 2.9 Å r.m.s.d. of the Cαs of the intermediate domain β sheet). This helix interacts both with the N-terminal domain and with the intermediate domain of its subunit, in particular with its β sheet. In curved tubulin, following rotation of this sheet, it also interacts with all of the colchicine domain ligands we have studied. Importantly, in $T_2R$ and in straight protofilaments, β-tubulin helix H8 is a major contributor to the intradimer intersubunit interface (4, 9).

When we initially determined the structure of colchicine bound to tubulin in $T_2R$, we identified the interaction of its N-acetyl appendage with the neighboring α-subunit and the steric hindrance that would result from the 2 subunits coming closer as in straight protofilaments as a major factor keeping the tubulin heterodimer in a curved conformation (4). The colchicine site binders we have studied here, some of which do not interact with the α-subunit, also prevent tubulin from adopting its straight structure; they make use of 2 additional mechanisms. When a colchicine domain molecule is bound to tubulin, the H7 and H8 α-helices, the T7 loop and the S8 and S9 β-strands, which contribute most to the core of the colchicine domain, all interact with the ligand. As a consequence, an effect of the colchicine domain compounds is to interfere with the concerted movements of these secondary structure elements required for tubulin to adopt its straight, microtubular conformation and, therefore, to assemble in microtubules (Fig. 4). In particular, colchicine domain ligands prevent the stacking of helix H8 onto the intermediate domain β sheet that is observed in microtubular tubulin. This disorganizes the intradimer interface and destabilizes the straight arrangement of tubulin subunits. The covalently bound T138067 reaches the same effect by preventing loop T7 from stacking on the intermediate domain β sheet as in microtubules (Fig. S2). In the case of TN16, additional interactions of this ligand with the N-terminal domain further contribute to the stability of the β-tubulin monomer in the curved conformation.

When tubulin is unliganded, the T7 loop takes the place of the colchicine site ligand, forces the H8 helix and the intermediate domain β sheet apart and prevents tubulin from adopting a straight conformation, as colchicine site ligands do. But, in this case, this effect is reversed as the T7 loop flips out of its curved tubulin location so that tubulin may switch between its curved and straight structures, as observed upon microtubule assembly. The localization of the T7 loop in soluble tubulin, in the absence of a colchicine domain ligand, opposes microtubule assembly suggesting that it contributes to microtubule dynamic instability. To be competent for assembly, tubulin has to be in the GTP state (i.e., with GTP bound to the β-subunit). There is increasing evidence that unassembled GTP-tubulin is curved, one of the most compelling arguments being that it binds allocolchicine and several other colchicine-domain ligands with an affinity very similar to that of GDP-tubulin (21, 22). The question then arises of how GTP favors tubulin assembly in microtubules. Although recent experimental results constrain the possible mechanisms (23), further work is required to determine the precise way in which GTP favors microtubular interactions and thereby tips the balance in favor of the tubulin straight conformation.

## Materials and Methods

**Proteins and Ligands.** Sheep brain tubulin was purified by 2 cycles of polymerization in a high molarity buffer followed by depolymerization (24) and finally stored at −70 °C in 50 mM Mes-K, pH 6.8, 33% glycerol, 0.25 mM $MgCl_2$, 0.5 mM EGTA, 0.1 mM GTP until use. Before preparation of the $T_2R$ complex, an additional microtubule assembly/disassembly cycle was performed. Tubulin concentrations were deduced from its absorbance ($\varepsilon_{278}$ = 1.2 mL $cm^{-1}$ $mg^{-1}$), assuming the molecular weight of the heterodimer is 100 kDa (25). The RB3 stathmin like domain (RB3-SLD) was expressed and purified as described (26). RB3-SLD concentration was determined by amino acid analysis or by titrating a known tubulin solution with RB3-SLD on a gel filtration column (Superose 12 10/300; Amersham). Both methods gave similar results.

ABT751 and T138067 were synthesized as described (27, 28). TN16 was purchased from Calbiochem. The bromo-derivative of ABT751 was synthesized according to the chemical route reported for the preparation of ABT751 and its analogs, using at the final step *p*-bromobenzenesulfonyl chloride instead of *p*-methoxybenzenesufonyl chloride for ABT751 (28).

**Crystallization of $T_2R$ and of $T_2R$-Colchicine Domain Compounds Complexes.** The colchicine domain compounds studied here were added to recycled tubulin (typically in the 50 to 80 μM concentration range) after it had been complexed with RB3-SLD as a $T_2R$ complex. T138067 and TN16 were added at a 250 μM, ABT751 at 400 μM, and its bromo-derivative at 150 μM final concentrations. The final DMSO concentration was 2% or lower. Complexes were concentrated to ≈20 mg tubulin/mL (100 μM $T_2R$) by ultrafiltration and were either used immediately or stored at −70 °C. Crystals were obtained at 4 °C by streak seeding (7).

**Data Collection and Refinement.** Crystals of $T_2R$ with or without small molecule ligands were flash-cooled in liquid nitrogen and diffraction datasets were collected at 100 K on beamlines ID14-eh4 and ID23-eh1 at the ESRF (Grenoble, France). Data were processed either with XDS (29) or with the HKL package (30). The $T_2R$-colchicine structure (PDB ID 1SA0) in which colchicine had been removed from the model was used as a starting point for refinement. The structures were refined with REFMAC (31) using the TLS option (32). Initial models and topology parameters for the ligands were generated using PRODRG (33). In the case of the $T_2R$ crystals (without a colchicine domain ligand), the highest signals in the Fobs-Fcalc maps (up to −7.5 σ) were localized on the T7 loop of each β-tubulin subunit, positive

peaks being located near the negative ones indicating the conformational change of this loop. Statistics for data processing and refinement are summarized in Table S1. We used the O program (34) for structure visualization and manual rebuilding. Superimpositions of atomic models were done either with SUPERPK (35) or with O (34). Figures were generated with PYMOL (36), BOBSCRIPT (37), MOLSCRIPT (38), and RASTER3D (39).

Additional details on the structure determination of $T_2$R-ligands complexes are given as *SI Materials and Methods*.

**ACKNOWLEDGMENTS.** Diffraction data were collected on beamlines ID14-eh4 and ID23-eh1 at the European Synchrotron Radiation Facility, Grenoble, France. This work was supported by La Ligue Contre Le Cancer (équipe labellisée 2006).

1. Mitchison T, Kirschner M (1984) Dynamic instability of microtubule growth. *Nature* 312:237–242.
2. Vandecandelaere A, Brune M, Webb MR, Martin SR, Bayley PM (1999) Phosphate release during microtubule assembly: What stabilizes growing microtubules? *Biochemistry* 38:8179–8188.
3. Lowe J, Li H, Downing KH, Nogales E (2001) Refined structure of $\alpha\beta$-tubulin at 3.5 A resolution. *J Mol Biol* 313:1045–1057.
4. Ravelli RBG, et al. (2004) Insight into tubulin regulation from a complex with colchicine and a stathmin-like domain. *Nature* 428:198–202.
5. Vandecandelaere A, Martin SR, Engelborghs Y (1997) Response of microtubules to the addition of colchicine and tubulin-colchicine: Evaluation of models for the interaction of drugs with microtubules. *Biochem J* 323:189–196.
6. Diaz JF, Andreu JM (1993) Assembly of purified GDP-tubulin into microtubules induced by taxol and taxotere: Reversibility, ligand stoichiometry, and competition. *Biochemistry* 32:2747–2755.
7. Dorleans A, Knossow M, Gigant B (2007) Studying drug-tubulin interactions by X-ray crystallography. *Methods Mol Med* 137:235–243.
8. Engelborghs Y (1998) General features of the recognition by tubulin of colchicine and related compounds. *Eur Biophys J* 27:437–445.
9. Nogales E, Whittaker M, Milligan RA, Downing KH (1999) High-resolution model of the microtubule. *Cell* 96:79–88.
10. Kiselyov A, Balakin KV, Tkachenko SE, Savchuk N, Ivachtchenko AV (2007) Recent progress in discovery and development of antimitotic agents. *Anticancer Agents Med Chem* 7:189–208.
11. Arai T (1983) Inhibition of microtubule assembly in vitro by TN-16, a synthetic antitumor drug. *FEBS Lett* 155:273–276.
12. Shan B, et al. (1999) Selective, covalent modification of $\beta$-tubulin residue Cys-239 by T138067, an antitumor agent with in vivo efficacy against multidrug-resistant tumors. *Proc Natl Acad Sci USA* 96:5686–5691.
13. Yoshimatsu K, Yamaguchi A, Yoshino H, Koyanagi N, Kitoh K (1997) Mechanism of action of E7010, an orally active sulfonamide antitumor agent: Inhibition of mitosis by binding to the colchicine site of tubulin. *Cancer Res* 57:3208–3213.
14. Mauer AM, et al. (2008) A phase II study of ABT-751 in patients with advanced non-small cell lung cancer. *J Thorac Oncol* 3:631–636.
15. Wang C, Cormier A, Gigant B, Knossow M (2007) Insight into the GTPase activity of tubulin from complexes with stathmin-like domains. *Biochemistry* 46:10595–10602.
16. Banerjee A, et al. (1988) A monoclonal antibody against the type II isotype of $\beta$-tubulin. Preparation of isotypically altered tubulin. *J Biol Chem* 263:3029–3034.
17. Cormier A, Marchand M, Ravelli RBG, Knossow M, Gigant B (2008) Structural insight into the inhibition of tubulin by vinca domain peptide ligands. *EMBO Rep* 9:1101–1106.
18. Kim do Y, et al. (2006) Design and biological evaluation of novel tubulin inhibitors as antimitotic agents using a pharmacophore binding model with tubulin. *J Med Chem* 49:5664–5670.
19. Li H, DeRosier DJ, Nicholson WV, Nogales E, Downing KH (2002) Microtubule structure at 8 Å resolution. *Structure* 10:1317–1328.
20. Gigant B, et al. (2000) The 4 Å X-ray structure of a tubulin:stathmin-like domain complex. *Cell* 102:809–816.
21. Rice LM, Montabana EA, Agard DA (2008) The lattice as allosteric effector: Structural studies of $\alpha\beta$- and $\lambda$-tubulin clarify the role of GTP in microtubule assembly. *Proc Natl Acad Sci USA* 105:5378–5383.
22. Shearwin KE, Timasheff SN (1994) Effect of colchicine analogues on the dissociation of $\alpha\beta$ tubulin into subunits: The locus of colchicine binding. *Biochemistry* 33:894–901.
23. Mozziconacci J, Sandblad L, Wachsmuth M, Brunner D, Karsenti E (2008) Tubulin dimers oligomerize before their incorporation into microtubules. *PLoS ONE* 3:e3821.
24. Castoldi M, Popov AV (2003) Purification of brain tubulin through two cycles of polymerization-depolymerization in a high-molarity buffer. *Protein Expr Purif* 32:83–88.
25. Correia JJ, Baty LT, Williams RC, Jr (1987) $Mg2+$ dependence of guanine nucleotide binding to tubulin. *J Biol Chem* 262:17278–17284.
26. Charbaut E, et al. (2001) Stathmin family proteins display specific molecular and tubulin binding properties. *J Biol Chem* 276:16146–16154.
27. Fei X, et al. (2004) Synthesis, biodistribution and micro-PET imaging of radiolabeled antimitotic agent T138067 analogues. *Bioorg Med Chem Lett* 14:1247–1251.
28. Yoshino H, et al. (1992) Novel sulfonamides as potential, systemically active antitumor agents. *J Med Chem* 35:2496–2497.
29. Kabsch W (1993) Automatic processing of rotation diffraction data from crystals of initially unknown symmetry and cell constants. *J Appl Cryst* 26:795–800.
30. Otwinowski Z, Minor W (1997) Processing of X-ray diffraction data collected in oscillation mode. *Methods Enzymol* 276:307–326.
31. CCP4 (1994) The CCP4 suite: Programs for protein crystallography. *Acta Crystallogr D Biol Crystallogr* 50:760–763.
32. Winn MD, Isupov MN, Murshudov GN (2001) Use of TLS parameters to model anisotropic displacements in macromolecular refinement. *Acta Crystallogr D Biol Crystallogr* 57:122–133.
33. Schuttelkopf AW, van Aalten DM (2004) PRODRG: A tool for high-throughput crystallography of protein-ligand complexes. *Acta Crystallogr D Biol Crystallogr* 60:1355–1363.
34. Jones TA, Zou JY, Cowan SW, Kjeldgaard M (1991) Improved methods for building protein models in electron density maps and the location of errors in these models. *Acta Crystallogr A* 47:110–119.
35. Dominguez R, et al. (1995) A common protein fold and similar active site in two distinct families of beta-glycanases. *Nat Struct Biol* 2:569–576.
36. DeLano WL (2002) *The PyMOL Molecular Graphics System*. (DeLano Scientific LLC, Palo Alto, CA).
37. Esnouf RM (1997) An extensively modified version of MolScript that includes greatly enhanced coloring capabilities. *J Mol Graphics* 15:133–138.
38. Kraulis P (1991) MOLSCRIPT: A program to produce both detailed and schematic plots of proteins structures. *J Appl Crystallogr* 24:946–950.
39. Meritt EA, Bacon DJ (1997) Raster3D: Photorealistic molecular graphics. *Methods Enzymol* 276:505–524.